ISSN 0021-3640, JETP Letters, 2017, Vol. 106, No. 9, pp. 582–586. © Pleiades Publishing, Inc., 2017.

CONDENSED MATTER

# Self-Consistent Mapping of the Ab Initio Calculations to the Multi-Orbital *p–d* Model: Magnetism in α-$FeSi_2$ Films as the Effect of the Local Environment[1]

**V. Zhandun[a, b, *], N. Zamkova[a], S. Ovchinnikov[a], and I. Sandalov[a]**

[a] *Kirensky Institute of Physics, Federal Research Center "Krasnoyarsk Science Centre, Siberian Branch of the Russian Academy of Sciences," Krasnoyarsk, 660036 Russia*

[b] *Reshetnev Siberian State Aerospace University, Krasnoyarsk, 660037 Russia*

**e-mail: jvc@iph.krasn.ru*

Received October 4, 2017

To accurately translate the results obtained within density functional theory (DFT) to the language of many-body theory we suggest and test the following approach: the parameters of the formulated model are to be found from the requirement that the model *self-consistent* electron density and density of electron states are as close as possible to the ones found from the DFT-based calculations. The investigation of the phase diagram of the model allows us to find the critical regions in magnetic properties. Then the behavior of the real system in these regions is checked by the ab initio calculations. As an example, we studied the physics of magnetic moment (MM) formation due to substitutions of Si by Fe-atoms or *vice versa* in the otherwise non-magnetic alloy α-$FeSi_2$. We find that the MM formation is essentially controlled by the interaction of Fe atoms with its *next* nearest atoms (NNN) and by their particular arrangement. The latter may result in different magnetic states *at the same concentrations* of constituents. Moreover, one of arrangements produces the counter-intuitive result: a ferromagnetism arises due to an increase in Si concentration in $Fe_{1-x}Si_{2+x}$ ordered alloy. The existing phenomenological models associate the destruction of magnetic moment only with the number of Fe–Si nearest neighbors. The presented results show that the crucial role in MM formation is played by the particular local NNN environment of the metal atom in the transition metal-metalloid alloy.

**DOI:** 10.1134/S0021364017210044

A need in a magnetic material that can be built into silicon-based semiconducting industry as well as a diversity of their possible phases supports inextinguishable interest to iron silicides. At the Fe-rich side of the binary phase diagram, metallic ferromagnets $Fe_5Si_3$ and $Fe_3Si$ have already been established as promising materials for spintronics. The Si-rich side of the phase diagram contains several variants of a disilicide stoichiometric compounds, such as the high-temperature tetragonal metallic α-$FeSi_2$ phase, with applications as an electrode or an interconnect material; the orthorhombic semiconducting β-$FeSi_2$ phase with direct band gap is an interesting candidate for thermoelectric and optoelectronic devices [1]. The iron silicides are also technologically advantageous since they can be grown epitaxially on many different semiconductor and insulator substrates [2–4]. The physical properties of the Fe–Si alloys in the film form can be drastically different from those of bulk. Furthermore, the Si-rich silicides, which do not exist in bulk, can be stabilized as films. What makes the system $Fe_xSi_{1-x}$ unique is that it allows for varying the degrees of both chemical and structural order over a wide composition range with the thin-film-growth techniques. One of the motivations for studying the Fe–Si system is the possibility to tune its magnetic properties. The experiments [5–7] on bulk $Fe_xSi_{1-x}$ alloys show that their magnetic properties strongly depend on Si concentration and chemical order. Most of the high-quality epitaxial films on Si exhibit ferromagnetism (FM). For example, the magnetic order is not observed in the bulk stoichiometric disilicide $FeSi_2$, however, the FM was found recently [8–10] in the α-$FeSi_2$, stabilized in the epitaxial-film form on the silicon substrate. The ferromagnetic phase of $Fe_5Si_3$ film at room temperature has been obtained recently [11], while the bulk $Fe_5Si_3$ is stable only at high temperature and is not magnetic. These experimental achievements have good perspective for the integration of the FeSi-based magnetic devices into silicon technology, and, therefore, demands for the detailed understanding of the physics of the MM formation in these compounds.

[1] The article is published in the original.

The local MM at Fe sites strongly depends on the distribution of Fe and Si neighbors and may either become higher than in pure iron or disappear at Si concentration of nearly 50%. The local environment effects are responsible for formation of high- and low-spin Fe species in the same compound. Experimentally, it was shown for ordered and disordered $Fe_xSi_{1-x}$ by neutron diffraction [12], the Mössbauer effect measurements [13, 14], and pulsed NMR studies [15]. Theoretically, the MM formation mechanism at Fe sites in Fe–Si alloys was discussed for more than half of a century. It is believed [13, 16–18] that the presence of the Si neighbors decreases the average magnetic moment at the Fe sites. The explanation of MM formation in iron silicides is given [13, 16–18] in terms of an *average* number of metallic or metalloid atoms in Fe nearest local environment. Whether the different spatial arrangements of Si atoms as well as the nearest (NN) and next nearest (NNN) local environments of Fe atoms may form different local MM on them or not remained unclear. Nevertheless, as stated in the works [7, 19] on Mössbauer spectra, the contribution of the NNN of Fe ions to MM formation on it seems to be far from negligible. Since it is difficult to extract from the ab initio density-functional based calculations the contributions from the local environment and simple models rarely reflect the features of a particular compound, we suggest to combine the ab initio calculations with the model ones by means of the following scheme. First, we perform the calculation of electronic and magnetic properties of the compound of interest within the framework of DFT-GGA for different way of silicon atoms substitution by iron atoms or *vice versa*. Then we perform mapping the DFT-GGA results to a model. The choice of the model is dictated by the facts that (i) the delocalized *d*-electrons are responsible for a magnetism in the Fe–Si alloys, and (ii) the intra-atomic Coulomb interactions are the largest matrix elements for them. These requirements lead us to the multiorbital Kanamory model with additional *d*–*d*-intersite exchange interaction between delocalized *d*-electrons. The parameters of the model should be found from the requirement that charge densities (as well as density of electron states), obtained *self-consistently* within the GGA-to-DFT and within the model calculations have to be as close to each other as possible. The model should help to clarify: (i) the mechanisms of local MM formation in iron silicides; (ii) the role played in it by the local environment. Our model contains five *d*-orbitals per spin for Fe atoms and three *p*-orbitals per spin for Si atom, takes into account all symmetries within the Slater–Koster scheme [20] and is solved in the Hartree–Fock approximation (HFA). The band structure arises due to hopping parameters, $t_1$(Fe–Fe) and $t_2$(Fe–Si) connect NN sites and $t_3$(Fe–Fe), $t_4$(Fe–Si) for the NNN sites. This way to perform the mapping, as far as we aware, has not been used before. Moreover, most of models do not take into account the NNN hoppings at all. The details of our model will be given elsewhere [21, 22]. As the criterion of the efficiency of the suggested way to model the system we choose the confirmation of the model calculations by the ab initio ones at different from the initial point in the parameter space. The crystal structure determines the local environment of ions and, therefore, the MM formation in the $\alpha$-$Fe_{1+x}Si_{2-x}$ alloys at increasing Fe concentration. The $\alpha$-$FeSi_2$ has a tetragonal structure ($P4/mmm$) with alternating Fe and Si layers perpendicular to tetragonal axis (Fig. 1a).

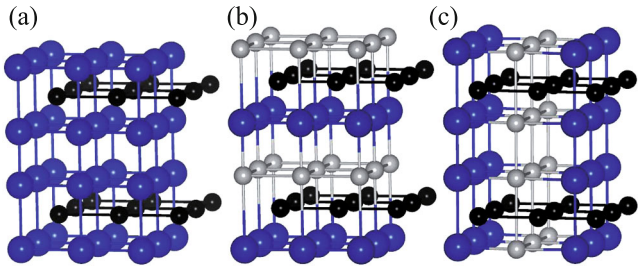


**Fig. 1.** (Color online) Structures of $\alpha$-$FeSi_2$ (a) and the ordered alloys (b, c). The Si atoms are shown by blue balls, the Fe atoms are indicated by grey balls, and the inserted $Fe_I$ atoms are shown by black balls with ab initio calculated magnetic moments. Optimized within GGA lattice parameters and the distance between NN and NNN Fe–Fe are shown in the second row. In L-type structure Fe atom has four Fe neighbors, whereas in C-type one only two Fe neighbors. (a) $\mu(Fe) = 0$, $a = b = 5.4$ Å, $c = 5.13$ Å; $R^{NNN}_{Fe-Fe} = 2.7$ Å; (b) L-type structure, $\mu(Fe) = 0$, $\mu(Fe_I) = 0$; $a = b = 5.07$ Å, $c = 5.37$ Å; $R^{NN}_{Fe-Fe} = 2.43$ Å, $R^{NNN}_{Fe-Fe} = 2.53$ Å; (c) C-type structure, $\mu(Fe) = 1.5\mu_B$, $\mu(Fe_I) = 2.5\mu_B$; $a = 5.13$ Å, $b = 5.56$ Å, $c = 5.37$ Å; $R^{NN}_{Fe-Fe} = 2.44$ Å, $R^{NNN}_{Fe-Fe} = 2.53$ Å, 2.78 Å.

The equilibrium lattice parameters, which are calculated in GGA, depend on the particular location of the Si atoms, which are substituted by Fe atoms at the same concentration of Fe. The case where four Si atoms are replaced by the Fe ones is shown in Figs. 1b and 1c. The values of Fe magnetic moments also strongly depend on spatial arrangement of $Fe_I$ atoms in local environment of Fe (Figs. 1b and 1c).The main difference between these two alloys' structures is the different distance between second Fe–Fe neighbors. Most important is the Fe–Fe-neighbors' interactions along the crystallographic axes. Indeed, the distance in the Fe layers between four NNN Fe–Fe pairs in the structure (L, Fig. 1b) is shorter than in the (C, Fig. 1c), correspondingly, we obtain zero local MM s in first the ordered alloy and non-zero local MM s in second one. Within our multiorbital model [21], rewritten for the present cases [22], the values of Fe local MM are determined mainly by the hopping term $t_3$, which connects NNN Fe–Fe.

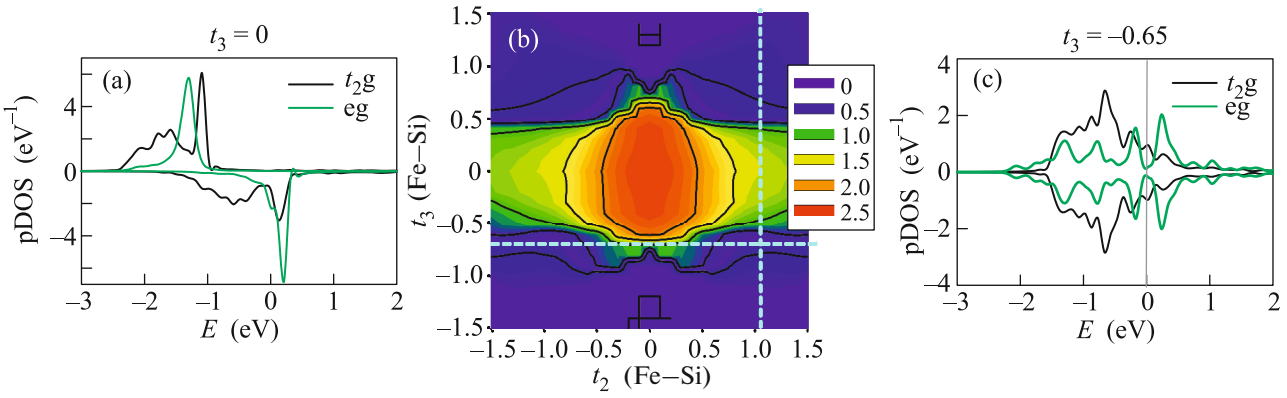


**Fig. 2.** (Color online) α-$FeSi_2$. (a) Model pDOS for zero value of hopping integral $t_3$(Fe–Fe) between NNN Fe–Fe. (b) Contour plot of Fe local MM dependence on hoppings $t_2$ between NN Fe–Si and $t_3$ between NNN Fe–Fe, the dashed line indicates the magnetic moment at the model hopping parameters. Different colors correspond to the values of the magnetic moments in Bohr magneton. (c) Model pDOS for hopping integral between NNN Fe–Fe $t_3$(Fe–Fe) = –0.65. All values of hopping integrals are given in Hubbard's-repulsion $U$ units.

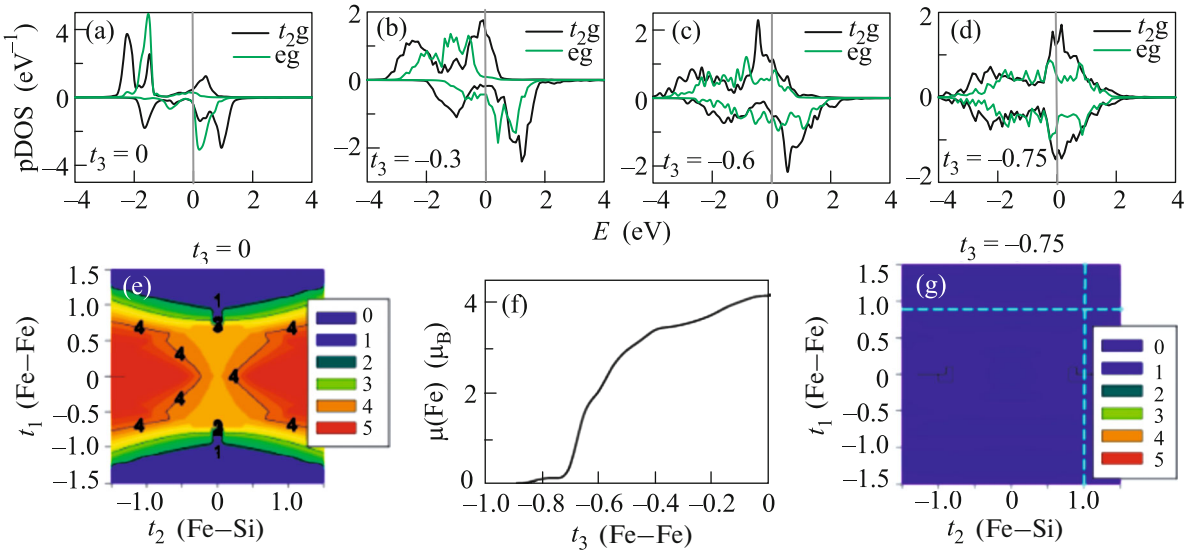


**Fig. 3.** (Color online) Alloy L. (a–d) Model pDOS for different values of NNN hopping integral $t_3$(Fe–Fe). (e, g) Contour plot of Fe local MM dependence on hoppings $t_1$ (between NN Fe–Fe) and $t_2$ (between NN Fe–Si) for hopping parameter between NNN Fe–Fe and $t_3$(Fe–Fe) = –0.75, correspondingly. (f) Dependence of magnetic moment on the hopping integral $t_3$ between NNN Fe–Fe. All values of hopping integrals are given in Hubbard $s$-repulsion $U$ units.

This is illustrated in Fig. 2, which shows the model partial DOS (pDOS) for Fe $d$-electrons of stoichiometric α-$FeSi_2$ at $t_3$(Fe–Fe) = 0 and $t_3$(Fe–Fe) = –0.65 (in Hubbard units $U$ [21, 22]) with the contour plot of Fe local MM. As seen, an increase in NNN $|t_3$(Fe–Fe)| leads to the formation of $d$-bands (c) from the $d$-levels (a). The region with magnetic states has very sharp boundaries (Fig. 2, local MM map), where the moment decreases till zero very fast. Notice that such a sharp boundary between magnetic and non-magnetic regions is the characteristic feature of all considered here iron silicides. For example, the effect of hopping $t_3$(Fe–Fe) can be seen in the change of the model pDOS and the map of the magnetic moments of substitution Fe atoms ($Fe_I$) in ordered alloy L (Fig. 3).

It is clear that, the gradual increase in $|t_3|$ first smoothly decreases local MM from the atomic like values and then at $|t_3| \simeq 0.6$ a sharp transition to the nonmagnetic state occurs.

Because the hopping integral $t_3$ is a function of the distance $R_{\text{Fe–Fe}}$, $t_3 = t_3(R_{\text{Fe–Fe}})$, this hopping in the

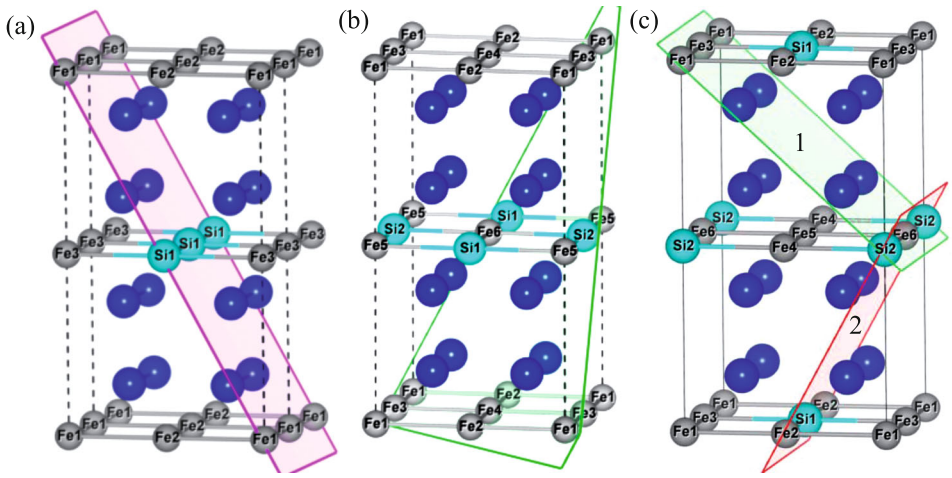


**Fig. 4.** (Color online) Different environments for Fe ions leading to MM formation when part of Fe ions are replaced by Si ions.

alloy C (Fig. 1b) should be less than that in the alloy L (Fig. 1c). This results in appearance of Fe local MM in the alloy C. Thus, we conclude from our model analysis that the Fe MM formation in the iron silicides are controlled by the number and the spacing of Fe–Fe couples in Fe layers. Notice that the existing theories [16–18] explained the increase in magnetic moment per unit cell by the increasing Fe concentration, which is correct only partly: it is possible to vary the number of Fe–Fe couples in Fe layers at the same concentration of Fe. Moreover, we can state [22] that the increase in the cell's magnetic moment with increase in $x$ in $\alpha$-$Fe_{1+x}Si_{2-x}$ alloys is associated namely with the appearance of high-spin Fe species in Si layers, which are surrounded mainly by Si. Thus, our model calculations lead to the conclusion that the Fe MM formation is controlled either by a decrease in the number of Fe–Fe couples in Fe layers or by an increase in the distance between Fe atoms in pairs. This condition can be fulfilled also *by an increase in the* Si concentration. In order to convince ourselves that this unexpected conclusion derived from the model is correct we carried out the ab initio GGA calculation of Fe magnetic moments for the ordered $\alpha$-$Fe_{1-x}Si_{2+x}$ alloys.

Figure 4 displays three different variants of substitution of Fe atoms in Fe planes by Si atoms. All calculations were carried out for the supercells $2a \times 2b \times 2c$ of $\alpha$-$FeSi_2$, which contain six iron atoms and two additional Si atoms. All considered alloys are magnetic, but the magnitude of the magnetic moment $\mu$ per unit cell (u.c.) depends on the particular positions (Figs. 4a–4c) of additional Si atoms: $\mu_{4a} = 3.4\mu_B$/u.c., $\mu_{4b} = 1.6\mu_B$/u.c., $\mu_{4c} = 3.3\mu_B$/u.c.. The magnitude of local MM on different Fe atoms corresponds to the expectations, derived from the model. Indeed, since the number of iron NNN surrounded $Fe_{III}$ atom is decreased by two, the local MM $\mu(Fe_{III}) \simeq 0.8\mu_B$ on $Fe_{III}$ arises. Similar local MM appear on $Fe_I$ and $Fe_V$ in the alloy (Fig. 4c) due to an increase in the distance between Fe–Fe NNN to 2.8 (see Fig. 1a). The alloy (Fig. 4b), however, presents an example where, it seems, the model is oversimplified: the GGA calculation produce zero moment on the $Fe_V$ atom without Fe atoms in NNN surrounding, while according to our model the local MM have to arise on the $Fe_V$ in this case. We assume that the missed term in the model responsible for this behavior is the crystal electric field (CEF), which is created by the Si surrounding: The $Fe_V$ in the alloy shown in Fig. 4b is sitting in most symmetrical local surrounding $P4/mmm$ by Si atoms, where the CEF splitting has to be stronger than in the (4a) and (4c) cases. In general, we may conclude that not only the increase in the Fe concentration can lead to the emergence of local MM on Fe atoms, but also of the metalloid concentration. The latter statement contradicts to the commonly accepted opinion that an increase in the magnetic moments in Fe–Si alloys can arise only due to an increase in the Fe concentration. According to our calculations the main role in MM formation in otherwise non-magnetic $\alpha$-$FeSi_2$ is played be a decrease in number of Fe–Fe pairs along the crystallographic axes and/or an increase in the distance between them. The latter can be done by either by fitting the lattice parameter of the substrate for $\alpha$-$FeSi_2$ film or by the substitution of Fe or Si atoms. As was pointed out in [9, 10], the best orientation relationships, that stabilize the epitaxial $\alpha$-$FeSi_2$ are $\alpha$-$FeSi_2(201) \parallel Si(110)$ or $\alpha$-$FeSi_2(110) \parallel Si(110)$. Such planes containing additional Si atoms are shown in Fig. 4: (a) (110) plane, (b) (111), (c) green (102) and red (101). Besides, as was reported in [8], the $\alpha$-$FeSi_2$ film was successfully stabilized with the orientation relationship $\alpha$-$FeSi_2(111) \parallel Si(001)$. For all alloys considered here, the sizes of (111) elementary cells are very

close to the Si(001)–(3 × 2) (11.5 Å × 7.68 Å): (11.83 Å × 7.89 Å), (11.76 Å × 7.83 Å), (11.67 Å × 7.93 Å) for the first (4a), second (4b), and third (4c) alloys, correspondingly, that gives the mismatch about −1.5%...−2.5%, which corresponds to the tensile strain of the α-$FeSi_2$(111) film.

Such a low mismatch presents an opportunity to stabilize the epitaxial films of the α-$FeSi_2$ structure. Similarly small mismatch has place also for the orientation α-$FeSi_2$(110) || Si(110).

The origin of magnetism in the α-$FeSi_2$(110) film was ascribed [8] to an increase in the Fe concentration. It remains unclear, however, where from the additional Fe atoms come. Here we propose the alternative explanation: the observed moment arises due to diffusion of the Si atoms to the film from the Si substrate and corresponding increase in Si concentration in the film. As was demonstrated above, certain types of local environment with increased Si concentration favor to MM formation. The magnetic moment $\mu \simeq 0.2–0.4\mu_B$/f.u. arises for all types of the substitutions shown in Fig. 4, and this is consistent with the observed in [8] values.

We are grateful to A.S. Shinkorenko for technical support. This work was supported by the Russian Foundation for Basic Research (project nos. 14-02-00186 and 17-02-00161) and by the Russian Foundation for Basic Research together with the Government of the Krasnoyarsk Territory (project nos. 16-42-243035, 16-42-242036, and 17-42-240212).

## REFERENCES

1. D. Leong, M. Harry, K. J. Reeson, and K. P. Homewood, Nature **387**, 686 (1997).
2. D. Berling, G. Gewinner, M. C. Hanf, K. Hricovini, S. Hong, B. Loegel, A. Mehdaoui, C. Pirri, M. H. Tuilier, and P. Wetzel, J. Magn. Magn. Mater. **191**, 331 (1999).
3. A. Ionescu, C. A. Vaz, T. Trypiniotis, C. M. Gurtler, H. Garsia-Miquel, J. A. C. Bland, M. E. Vickers, R. M. Dalgliesh, C. Langridge, Y. Bugoslavsky, Y. Miyoshi, L. F. Cohen, and K. R. A. Ziebeck, Phys. Rev. B **71**, 094401 (2005).
4. M. Walterfang, W. Keune, K. Trounov, R. Peters, U. Rucker, and K. Westerholt, Phys. Rev. B **73**, 214423 (2006).
5. A. X. Gray, J. Karel, J. Min'ar, C. Bordel, H. Ebert, J. Braun, S. Ueda, Y. Yamashita, L. Ouyang, D. J. Smith, K. Kobayashi, F. Hellman, and C. S. Fadley, Phys. Rev. B **83**, 195112 (2011).
6. G. Bertotti, A. R. Ferchmin, E. Fiorillo, K. Fukamichi, K. Kobe, and S. Roth, *Soft Magnetic Allows. Invar and Elinvar Allows,* Subvol. 1: *Magnetic Allows for Technical Applications* (Springer, Berlin, 1994), p. 33.
7. V. A. Niculescu, T. J. Burch, and J. I. Budnick, J. Magn. Magn. Mater. **39**, 223 (1983).
8. G. Cao, D. J. Singh, X.-G. Zhang, G. Samolyuk, L. Qiao, C. Parish, K. Jin, Y. Zhang, H. Guo, S. Tang, W. Wang, J. Yi, C. Cantoni, W. Siemons, E. A. Payzant, M. Biegalski, T. Z. Ward, D. Mandrus, G. M. Stocks, and Z. Gai, Phys. Rev. Lett. **114**, 147202 (2015).
9. J. K. Tripathi, M. Garbrecht, W. D. Kaplan, G. Markovich, and I. Goldfarb, Nanotechnology **23**, 495603 (2012).
10. J. K. Tripathi, G. Markovich, and I. Goldfarb, Appl. Phys. Lett. **102**, 251604 (2013).
11. S. A. Lyaschenko, Z. I. Popov, S. N. Varnakov, L. A. Kuzubov, S. G. Ovchinnikov, T. S. Shamirzaev, A. V. Latyshev, and A. A. Saranin, J. Exp. Theor. Phys. **120**, 886 (2015).
12. S. Yoon and J. G. Booth, Phys. Rev. Lett. A **48**, 381 (1974).
13. A. K. Arzhnikov, L. V. Dobysheva, G. N. Konygin, E. V. Voronina, and E. P. Yelsukov, Phys. Rev. B **65**, 024419 (2001).
14. T. J. Burch, T. Litrenta, and J. I. Budnick, Phys. Rev. Lett. **33**, 421 (1974).
15. M. B. Stearns, Phys. Rev. B **4**, 4069 (1971).
16. W. A. Hines, A. H. Menotti, J. I. Budnick, T. J. Burch, T. Litrenta, V. Niculescu, and K. Ray, Phys. Rev. B **13**, 4060 (1976).
17. E. P. Elsukov, G. N. Konygin, V. A. Barinov, and E. V. Voronina, J. Phys.: Condens. Matter **4**, 7597 (1992).
18. J. Kudrnovsky, N. E. Christensen, and O. K. Andersen, Phys. Rev. B **43**, 5924 (1991).
19. E. Voronina, T. Miyanaga, A. Deyev, V. Kriventsov, G. Konygin, and E. Yelsukov, Nucl. Instrum. Methods Phys. Res. A **575**, 189 (2007).
20. J. C. Slater and G. F. Koster, Phys. Rev. **94**, 1498 (1954).
21. N. G. Zamkova, V. S. Zhandun, S. G. Ovchinnikov, and I. S. Sandalov, J. Alloys Compd. **695**, 1213 (2017).
22. V. S. Zhandun, N. G. Zamkova, S. G. Ovchinnikov, and I. S. Sandalov, Phys. Rev. B **95**, 054429 (2017).